Combination of the Monte Carlo approach and the Helming method to simulate abnormal grain growth

T. Baudin[1,2]*, R. Penelle[1,2], D. Ceccaldi[1,2]

[1] *CNRS, UMR8182, ICMMO, Laboratoire de Physico-Chimie de l'Etat Solide, Orsay, F-91405, France*
[2] *Univ Paris-Sud 11, Orsay, F-91405, France*

Received 9 May 2008, received in revised form 23 July 2008, accepted 28 July 2008

Abstract

The Helming method is employed to improve the definition of the orientation classes used to define the crystallographic texture in abnormal grain growth simulation. It involves fitting the experimental texture measured by X-ray or neutron diffraction by several orientations modelled by Gaussian functions. The orientation classes are then used to describe the distribution of grain boundary energy on experimental microstructures characterized by EBSD (Electron Back Scattered Diffraction) and introduced as input data into the simulation. The approach is tested in the case of the Monte Carlo simulation of abnormal growth of Goss grains in a Fe3%Si sheet. The results are compared with those obtained through classical methods which arbitrarily impose spreading around the main texture components. Finally, it appears that the evolution of their volume fraction during the simulation is very sensitive to the definition of the orientation classes.

K e y w o r d s: texture components, abnormal grain growth, Monte Carlo simulation, grain boundary energy

1. Introduction

The occurrence of secondary recrystallization in a microstructure where primary recrystallization is complete depends on several parameters [1, 2] and has been notably simulated using Monte Carlo techniques [3–8].

One phenomenon is the pre-existence of grains that are larger than the average size of the matrix grains. Another one is the influence of the particles on the growth process. Such phenomena have been observed for example in nickel-based superalloys produced by powder metallurgy techniques for high temperature applications [9–11].

In some materials, however, the size advantage is not observed. In this case, the abnormal growth can develop through anisotropy of the grain boundary (GB) energy and mobility, since these last quantities depend on the misorientation between grains [12–14]. This idea has motivated the development of models in which mobility and interfacial energy of the growing grain are taken into account (see [5, 15, 16]).

The energy and mobility of all the GB present in the polycrystal must then be experimentally discovered for each material studied. This involves a great deal of experimental work and this is generally why the crystallographic orientation number (as well as the number of GB types) is decreased. For example, Rollet et al. [5] used only 2 texture components, Abbruzzese et al. [17] and Baudin et al. [18] considered 3 texture components, Paillard et al. [19] 4 texture components... Kunaver and Kolar [20] have proposed a three-dimensional computer simulation of anisotropic grain growth in ceramics. For that purpose, they separated the grains into two distinct classes: the matrix (normal growth) and the grains whose growth was anisotropic. The grain boundaries exhibit a high energy in one direction and a lower energy in the others.

This work describes an intermediary approach, which involves the use of more than 3 or 4 texture components but without taking into account the complete orientation space. Indeed, it seems evident that the *texture component number* and their *volume frac-*

*Corresponding author: tel.: +33 (0)1 69157983; fax: +33 (0)1 69154797; e-mail address: Thierry.Baudin@u-psud.fr

tion (which is linked to their spreading) affect the simulation results.

2. Abnormal grain growth simulation

The Monte Carlo simulation principle has already been described elsewhere [19]. The simulation is performed from experimental data [21] characterized by Orientation Imaging Microscopy (OIM^{TM}) [22]: the orientations are automatically measured by EBSD [23] at each point of a hexagonal grid and the microstructure is then reconstructed from the orientation measurements.

To test the influence of the texture component number and their spreading on the simulation of the abnormal growth, the Fe3%Si alloy was chosen because of the large amount of existing experimental data and because abnormal growth is still studied in such a material (see for example [24–26]).

Most transformer cores are made of Fe3%Si (HiB or GO grades) textured sheets, which minimize Watt losses thanks to the presence of the $\{110\}\langle001\rangle$ Goss texture where the easiest magnetization directions $\langle001\rangle$ are parallel to the magnetic field direction. Development of such a texture occurs by abnormal growth of a minority of Goss grains present in the primary recrystallized matrix. If the industrial processing has been improved over these last few decades, the mechanisms of the Goss secondary recrystallization texture development are not well established [24]. However, with the different approaches, the nature of grain boundary (misorientation and rotation axis, the GB plane is not taken into account) plays an important role in their mobility. For example, a theory assumes that the boundaries of Goss oriented grains are more often of the coincident site lattice (CSL) type than other types of grain boundaries. Moreover, in the presence of precipitates, the CSL boundaries are supposed to be less dragged than the general boundaries. The Goss grains can then grow faster than the others.

Keep in mind that in this paper the possible mechanisms for the abnormal growth are not discussed. In fact, the material is only chosen for convenience purposes in order to show the feasibility and the interest of the proposed approach that mainly consists in defining the orientation classes and so the texture used in the simulations.

After primary recrystallization (Fig. 1), the average grain diameter is quite small (about 15 μm) and therefore to have a sufficient grain number (> 1000) [27, 28], the measured area with EBSD is a square of 450×450 μm, the step size being equal to 2 μm. The primary recrystallization texture is composed of the $\{111\}\langle112\rangle$ main component and the $\{100\}\langle012\rangle$ secondary component (see for example [29]).

Since the growth rate depends on the mobility and the energy of grain boundaries, in a previous study [30], the values (Table 1) used to simulate the abnormal grain growth were chosen from those proposed by Abbruzzese et al. [6] (see [19]). These values have arbitrary units and have been classified to reproduce the experimental observations, i.e. the growth of the Goss grains.

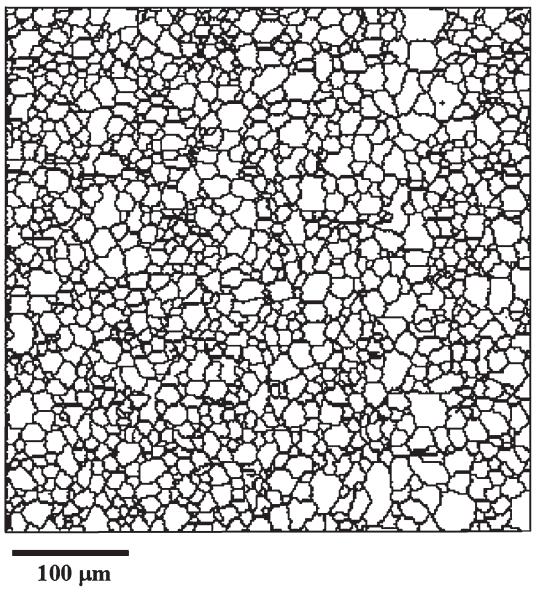

Fig. 1. Fe3%Si (grade HiB) – experimental microstructure after primary recrystallization analysed by OIM and reconstructed from the grain boundary description.

From these data, several simulations were initially performed to test the influence of the texture component number and their spreading on the simulation results.

2.1. Effects of the texture component number on the simulation results

Let us assume that the initial microstructure of Fe3%Si sheet is composed of four components: the Goss component $\{110\}\langle001\rangle$ with a 6° spreading (which allows us to find Goss grains in the microstructure, see [30]), the $\{111\}\langle112\rangle$ and $\{100\}\langle012\rangle$ components with a 25° spreading and the random part of the initial texture. Figure 2 shows the volume fraction evolution of each component during the simulation. Then, the same calculation is reproduced but with only three components, so the $\{100\}\langle012\rangle$ component is introduced into the random part.

Figure 2 allows us to compare the results obtained with the two calculations and shows that they converge to the same values. Indeed, in each case the Goss grains abnormally grow and the other components disappear. However, several important differences should be noted.

Table 1. Energy and mobility coefficients (arbitrary values)

Boundary type	{110}⟨001⟩ {111}⟨112⟩	{110}⟨001⟩ {100}⟨012⟩	{110}⟨001⟩ Random	{111}⟨112⟩ {100}⟨012⟩	{111}⟨112⟩ Random	{100}⟨012⟩ Random
Energy	330	260	300	360	380	350
Mobility	2.5	0.1	2.5	2.3	2.5	2.5

Boundary type	{110}⟨001⟩ {110}⟨001⟩	{111}⟨112⟩ {111}⟨112⟩	{100}⟨012⟩ {100}⟨012⟩	Random Random
Energy	400	450	600	650
Mobility	0.1	0.2	0.1	0.4

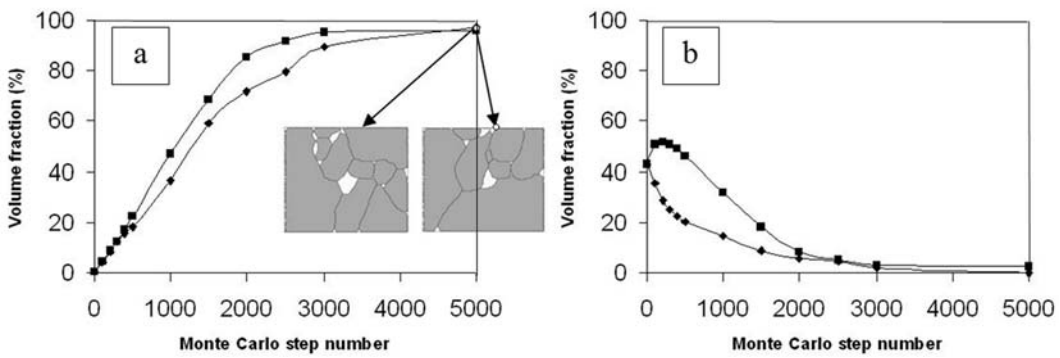

Fig. 2. Evolution of the volume fraction of (a) the Goss and (b) {111}⟨112⟩ orientation classes during the simulation (◆) with 4 or (■) 3 texture components. The final simulated microstructures are presented on Fig. 2a (the grey grains are the Goss grains).

With the second calculation (3 components), the {111}⟨112⟩ component begins to grow and then disappears. Consequently, the recrystallization mechanism (in the simulation) is not the same and the final microstructure can be different as verified for this example. Indeed, at the end of the simulation, the grain number (and the grain shape) is not the same and consequently, the physical properties of the material can be different.

2.2. Effects of texture component spreading on the simulation results

An abnormal growth kinetics is also modified by spreading of the chosen texture components. Indeed, each texture component or orientation class must be characterized by the orientation and spreading around this orientation. The same initial microstructure of the Fe3%Si sheet is characterized by the 4 components described above, but the spreading of the {111}⟨112⟩ and {100}⟨012⟩ orientations is chosen equal to 15° for the first calculation and 25° for the second calculation. Firstly, it is verified that the final grain number is obviously not the same. Moreover, the texture components evolve with the orientation spread as shown in Fig. 3. The difference is particularly visible for the {111}⟨112⟩ component since its volume fraction continuously decreases for a calculation, whereas a normal growth is observed in the first steps of the other calculation.

These simple examples show that the choice of the component number and their shape (half the width of the corresponding gaussian functions) are important parameters in abnormal growth simulation, also knowing that the experimental mechanisms are often not well known. However, for such a calculation, the number of variables (i.e. the number of texture components) must stay quite low and it must be sufficient to give a good texture description which is possible with the component methods [31, 32].

3. Determination of orientation classes

The texture was measured on the surface of the Fe3%Si sheet (grade HiB) with a thickness of 320 μm after primary recrystallization by X-ray diffraction in reflexion-transmission to have complete pole figures [29]. Assuming the sample orthotropic symmetry, the even part of the Orientation Distribution Function (ODF) is calculated using the harmonic method ($L = 22$) and the total ODF $F(g)$ is determined using the positivity method (see [27]).

As discussed above, the two main components near

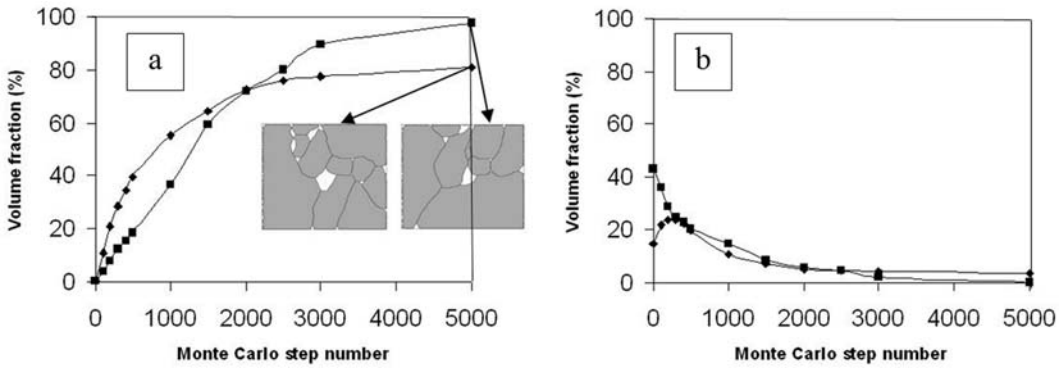

Fig. 3. Evolution of the volume fraction of (a) the Goss and (b) $\{111\}\langle 112\rangle$ orientation classes during the simulation with (◆) 15° spreading and (■) 25° spreading for the $\{111\}\langle 112\rangle$ and $\{100\}\langle 012\rangle$ orientations.

Table 2. Comparison of the component volume fraction estimated with the Rouag and the Abbruzzese approaches

	$\{111\}\langle 112\rangle$	$\{100\}\langle 012\rangle$
Rouag approach	50.0 %	20.0 %
Abbruzzese approach	22.0 %	8.5 %

$\{111\}\langle 112\rangle$ and $\{100\}\langle 012\rangle$ can be used to characterize the sheet texture. Regarding the volume fraction of the texture components, Rouag [33] initially mentioned that the Goss orientation is undetected by X-ray diffraction which means that its volume fraction is less than 5 % for the HiB grade: an estimate from metallographic observations leads to about 10^{-2} %. However, this estimation is an average since the presence of Goss clusters can locally modify this percentage [21]. Secondly, Rouag [33] estimated the volume fraction of the two main components from the ODF calculation and found the values given in Table 2. This volume fraction is calculated by discrete summation of elementary volume fractions defined in the Euler space for each domain ($\Delta\psi = \Delta\theta = \Delta\phi = 5°$ with the Roe notation [34]), on all the retained orientations in the equivalent tubes which define the two main components. In this calculation, the minimal ODF value is set at 1.

In another approach, Abbruzzese et al. [6] used a 15° conic dispersion around ND (Normal Direction) for the $\{111\}\langle 112\rangle$ component for their grain growth simulation. Moreover, they defined the Goss component with two classes: the Goss grains ±5° around RD (Rolling Direction) and the grains from ±5° up to ±15° around both $\langle 001\rangle$//RD and $\langle 110\rangle$//ND.

To simplify the comparison with the Rouag approach, the Abbruzzese type calculations are performed with the same orientation classes, each of them being defined by a spreading of 15° around the ideal components except for the random class. Table 2 shows that the results obtained with the two different approaches are very different and consequently, the simulations give very different simulated microstructures (see for example [21]).

The Rouag approach does not seem realistic since it leads to a great deal of dispersion around the $\{111\}\langle 112\rangle$ and $\{100\}\langle 012\rangle$ components. Thus, if a sphere is centered on the ideal orientations of $\{111\}\langle 112\rangle$ and $\{100\}\langle 012\rangle$ that define the corresponding classes, the maximum misorientation between a given orientation inside the class and the ideal orientation must reach about 30° and 22° respectively to meet the volume fraction given in Table 2. The same problem is observed with the Abbruzzese approach for the random class that becomes very large since the dispersion around the main components is quite low.

Thus both approaches described previously are not satisfactory and the texture description must therefore be improved. The component method can be used to do that. This method allows us to describe a texture by only several components that can be defined from an ODF calculation [32] or directly from the experimental pole figures [31]. Using this last one, i.e. the Helming method, the texture is fitted by 12 components modelled by Gaussian functions (Table 3), with the background (fon) value being approximately equal to zero. Note that the calculation has been performed assuming the orthotropic symmetry of the texture. For future applications to particular materials it could be important to use the triclinic symmetry of the texture. This modification simply involves increasing the orientation class number and taking into account the multiplicity of the ideal orientations characterizing the classes.

The ODF can be calculated as the sum of the 12 Gaussian functions. Since the total ODF determined from X-ray measurements is calculated using the harmonic method (Fig. 4), this last method is used with the same series expansion order, $L = 22$. Figures 4c,d show that this procedure allows to reproduce the total ODF (Figs. 4a,b) knowing that the fit could be im-

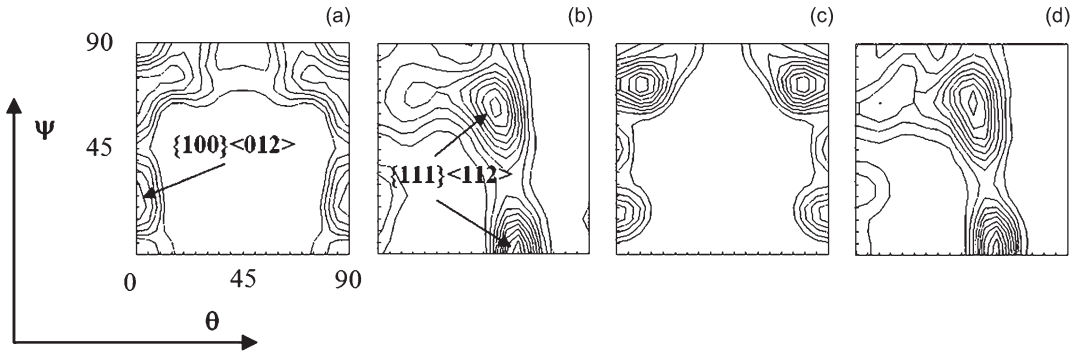

Fig. 4. ODF calculated from pole figures measured by X-ray diffraction: (a) $\varphi = 0°$ (intensity levels at 1, 1.4, 1.8, 2.2, 2.6) and (b) $\varphi = 45°$ (intensity levels at 1, 2, ..., 11) ODF section plot. ODF calculated from the 12 components defined in Table 3: (c) $\varphi = 0°$ (intensity levels at 1, 1.4, ..., 3.8) and (d) $\varphi = 45°$ (intensity levels at 1, 2, ..., 10) ODF section plot.

Table 3. Definition of the 12 components determined with the Helming method

Texture components				Gaussian functions	
Number	ψ (°)	θ(°)	φ (°)	Half width (°)	Weight
1	55.2	58.2	124.7	13.8	18.4
2	2.0	59.0	138.9	12.7	12.6
3	248.9	64.9	112.9	15.3	11.0
4	86.3	67.4	33.3	18.6	5.1
5	323.0	54.7	136.0	10.8	2.6
6	135.0	52.5	134.5	9.2	2.5
7	205.9	60.4	128.6	10.5	1.3
8	266.3	43.1	43.4	11.0	0.9
9	342.7	85.5	168.3	19.5	27.1
10	39.8	92.3	178.1	8.0	0.9
11	30.8	74.5	106.7	16.8	11.9
12	87.1	119.8	95.8	17.0	5.7

Table 4. Comparison of the component volume fraction estimated with the Rouag and the Helming approaches

	$\{111\}\langle 112\rangle$	$\{100\}\langle 012\rangle$
Rouag approach	50.0 %	20.0 %
Helming approach	54.4 %	28.0 %

proved by increasing the component number to define the $\{100\}\langle 012\rangle$ component. Indeed, as the $\{111\}\langle 112\rangle$ component seems to play the most important role in the abnormal growth theories [24], it has to be well fitted.

All the components defined in Table 3 can be assigned to one of the orientation classes defined above, therefore the components 1 to 8 can be assigned to the $\{111\}\langle 112\rangle$ class, the components 9 and 10 to the $\{100\}\langle 012\rangle$ class and the components 11 and 12 to the random class. Then, the volume fraction of each orientation class can be calculated and compared to those estimated with the Rouag approach (Table 4).

Table 4 shows a good agreement between the results obtained with the two different approaches. As explained previously, the more important difference is observed in the $\{100\}\langle 012\rangle$ class which is overestimated by using only two components.

The influence of the initial texture description on the simulated microstructure during abnormal grain growth must now be tested.

4. Abnormal grain growth simulation using the texture components determined with the Helming method

4.1. Choice of the energy and mobility values

The energy and mobility values described in Table 1 are maintained. However, a spreading is introduced (Table 5) to take into account the orientation sub-classes as described in the next section.

Because the orientation number has increased using the Helming method (12 components, see Table 3), the energy and mobility coefficients need to be adjus-

Table 5. Energy coefficients (arbitrary values)

Boundary type	{110}⟨001⟩ {111}⟨112⟩	{110}⟨001⟩ {100}⟨012⟩	{110}⟨001⟩ Random	{111}⟨112⟩ {100}⟨012⟩	{111}⟨112⟩ Random	{100}⟨012⟩ Random
Energy	330–301	260–231	300–261	360–351	380–361	350–331
Boundary type	{110}⟨001⟩ {110}⟨001⟩	{111}⟨112⟩ {111}⟨112⟩	{100}⟨012⟩ {100}⟨012⟩	Random Random		
Energy	400	450-420	600-570	650		

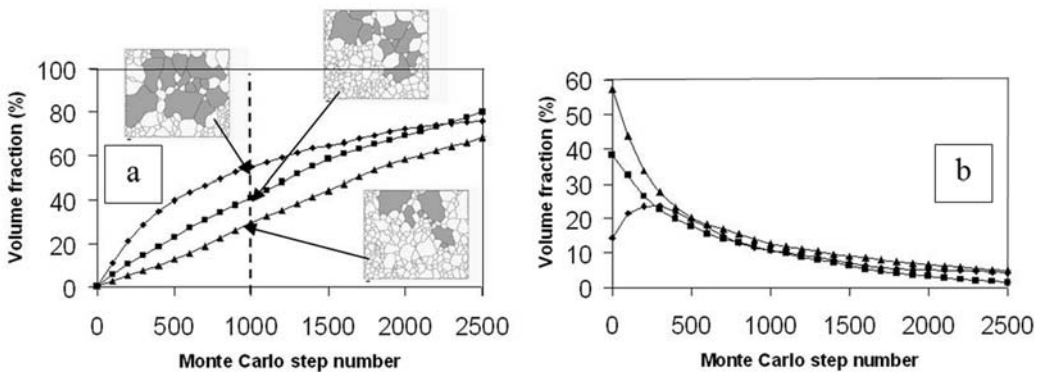

Fig. 5. Evolution of the volume fraction of (a) Goss grains and (b) {111}⟨112⟩ grains during the simulation: (◆) LS approach, (■) IS approach, (▲) HS approach. The corresponding microstructures obtained for 1000 MCS are presented. The grey grains are the Goss grains.

ted. For that, a simplified approach is proposed:

(i) The mobility values defined in Table 1 are kept and only the energy values are modified.

(ii) As previously mentioned, an orientation class is composed of several components (see Table 3). The {111}⟨112⟩ class is therefore defined by the sum of 8 texture components or 8 sub-classes and the {100}⟨012⟩ and the random classes are characterized by 2 sub-classes.

(iii) The energy between two defined orientation classes is not characterized by one value (see Table 1) but by an energy range between $E_{\max}$ and $E_{\min}$ as given in Table 5.

(iv) To calculate the GB energy value (E) between two grains, their orientation is firstly associated to the corresponding orientation classes or sub-classes. Since the relationship between E and the misorientation ($\Delta\theta$) between these two orientations is not experimentally known, E is then defined by a linear evolution in the range between $E_{\max}$ and $E_{\min}$ as a function of $\Delta\theta$. This linear relationship is obviously oversimplified.

4.2. Abnormal grain growth simulation results

The three Abbruzzese, Rouag and Helming approaches will now be respectively named Low, High and Intermediary Spreading approaches, or LS, HS and IS approaches. Here the HS approach is not perfectly applied since spheres centered on the ideal orientations that define the classes are used with a spreading of 30° and 22° respectively for the {111}⟨112⟩ and {100}⟨012⟩ components as described above.

Starting from the EBSD map (Fig. 1) as initial input data, the Monte Carlo simulation has been performed to 2500 Monte Carlo steps (MCS). This number has been chosen as a function of the Goss grain size. Indeed, when the Goss grains become very large, they are cut off by the microstructure limits. Such a microstructure cannot be quantitatively interpreted since the grain size is indeterminate. Because the Goss component evolution is the most interesting and because the {111}⟨112⟩ orientation is well fitted (unlike the {100}⟨012⟩ orientation class), only the volume fraction evolution of these two components during the simulation is discussed. With regard to the two other orientation classes, i.e. {100}⟨012⟩ and random ones, the curves are not very different from those described by Paillard et al. [19]. There is normal growth of the {100}⟨012⟩ grains at the beginning of the simulation before a decrease when the Goss grains consume these grains.

Figures 5a and 5b respectively show the evolution of the {110}⟨001⟩ and {111}⟨112⟩ components during the abnormal growth simulation.

These curves have been calculated using the three

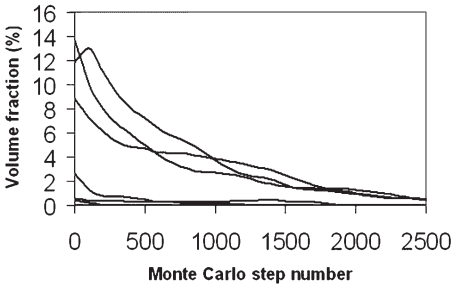

Fig. 6. Evolution of the volume fraction of $\{111\}\langle 112\rangle$ grains defined by the 8 sub-classes described in Table 3) (several curves are superimposed at level 0 of the volume fraction).

LS, HS and IS approaches. The simulated microstructures are very different as seen in Fig. 5a for 1000 Monte Carlo steps. It can be said that the Goss grain number as well as the Goss volume fraction can be very different in the three simulations. These examples prove the necessity to correctly choose the orientation classes to provide an accurate description of the final microstructure after secondary recrystallization.

For the $\{111\}\langle 112\rangle$ component, the HS approach obviously leads to the highest volume fractions. Instead, the two other approaches give similar results at least when the MCS number is greater than about 300. Below this limit, the LS approach shows an increase of the volume fraction of grains having this orientation that is not observed on the other curves.

With the IS approach, the $\{111\}\langle 112\rangle$ volume fraction is calculated as the sum of the 8 sub-classes. However, it is possible to follow the evolution of the volume fraction of each sub-class as described in Fig. 6.

Therefore, it appears that all the components have not the same behaviour since there is an increase in one of them with the IS approach (Fig. 6). This component obviously corresponds to a near orientation class used with the LS approach. So with the IS approach, the behaviour of the different texture components inside the orientation classes generally used in the literature can be described more precisely.

Let us note that Figs. 5 and 6 show differences over brief periods of time due to the chosen approaches, but a convergence appears for long periods of time. For these last conditions, the microstructure is composed of a very limited grain number depending on the initial Goss volume fraction after primary recrystallization. The simulation of brief times is however very important since it can be useful to better understand the possible abnormal growth mechanisms which are still not understood very well from an experimental point of view [24]. In order to precisely reproduce the texture, it is interesting to use the Helming method to reproduce the mechanisms during the secondary recrystallization.

5. Conclusion

This study, using the Helming component method, is an attempt to improve the texture description to be used in the abnormal growth simulations. The Monte Carlo simulation has been applied here but this problem remains for all the other types of simulation such as the cellular automaton model or the vertex model. In its principle, the approach only involves increasing the orientation class number. Consequently, the simulation results obtained by the combination of the Helming method and the Monte Carlo simulation, are obviously better than those obtained by the classical simulations.

To become predictive, such calculation should take into account experimental energy and mobility values. Measurements on bicrystals or tricrystals would then need to be taken. Another approach could involve adjusting these parameters by comparing numerical and experimental results, this comparison being facilitated since the simulation is performed using experimental data.

References

[1] HUMPHREYS, F. J.—HATERLY, M.: Recrystallization and Related Annealing Phenomena. Oxford, Elsevier 2004.
[2] RIOS, P.: In: Proceedings of the first joint international conference on recrystallization and grain growth. Eds.: Gottstein, G., Molodov, D. A. Berlin, Springer Verlag 2001, p. 115.
[3] ANDERSON, M. P.—SROLOVITZ, D. J.—GREST, G. S.—SAHNI, P. S.: Acta Metall., *32*, 1984, p. 783.
[4] SROLOVITZ, D. J.—ANDERSON, M. P.—SAHNI, P. S.—GREST, G. S.: Acta Metall., *32*, 1984, p. 793.
[5] ROLLETT, A. D.—SROLOVITZ, D. J.—ANDERSON, M. P.: Acta Metallurgica, *37*, 1989, p. 1227.
[6] ABBRUZZESE, G.—CAMPOPIANO, A.—FORTUNATI, S.: Textures and Microstructures, *14–18*, 1991, p. 775.
[7] IVASISHIN, O. M.—SHEVCHENKO, S. V.—SEMIATIN, S. L.: Scripta Materialia, *50*, 2004, p. 1241.
[8] MORHÁČOVÁ, E.—MORHÁČ, M.: Kovove Mater., *45*, 2007, p. 105.
[9] MESSINA, R.—SOUCAIL, M.— BAUDIN, T.—KUBIN, L.: J. of Applied Physics, *84*, 1998, p. 6366.
[10] MESSINA, R.—SOUCAIL, M.— KUBIN, L.: Mat. Sci. and Eng., *A308*, 2001, p. 258.
[11] SOUCAIL, M.—MESSINA, R.—COSNUAU, A.—KUBIN, L. P.: Mat. Sci. and Eng., *A271*, 1999, p. 1.
[12] NOVIKOV, V.: Grain growth and control of microstructure and texture in polycrystalline materials. Boca Raton, Florida, CRC Press 1997.
[13] GOTTSTEIN, G.—SHVINDLERMAN, L. S.: Grain boundary migration in metals – Thermodynamics, kinetics, applications. Boca Raton, Florida, CRC Press 1999.
[14] PRIESTER, L.: Les joints de grains – De la théorie à l'ingénierie. Les Ulis, EDP Sciences 2006.

[15] ROLLET, A. D.—MULLINS, W. W.: Scripta Materialia, *36*, 1997, p. 975.
[16] CALEYO, F.—BAUDIN, T.—PENELLE, R.: Scripta Materialia, *46*, 2002, p. 829.
[17] ABBRUZZESE, G.—FORTUNATI, S.—CAMPOPIANO, A.: Mat. Sci. Forum, *94–96*, 1992, p. 405.
[18] BAUDIN, T.—JULLIARD, F.—PAILLARD, P.—PENELLE, R.: Scripta Materialia, *43*, 2000, p. 63.
[19] PAILLARD, P.—BAUDIN, T.—PENELLE, R.: Mat. Sci. Forum, *157–162*, 1994, p. 1847.
[20] KUNAVER, U.—KOLAR, D.: Acta Mater., *46*, 1998, p. 4629.
[21] BAUDIN, T.—PAILLARD, P.—PENELLE, R.: Scripta Materialia, *36*, 1997, p. 789.
[22] ADAMS, B. L.—WRIGHT, S. I.—KUNZE, K.: Met. Trans. A, *24A*, 1993, p. 819.
[23] DINGLEY, D. J.: Scanning Electron Microscopy, *4*, 1981, p. 273.
[24] MORAWIEC, A.: Scripta Materialia, *43*, 2000, p. 275.
[25] ETTER, A. L.—BAUDIN, T.—PENELLE, R.: Scripta Materialia, *47*, 2002, p. 725.
[26] MAAZI, N.—ROUAG, N.—ETTER, A. L.—PENELLE, R.—BAUDIN, T.: Scripta Materialia, *55*, 2006, p. 641.
[27] BAUDIN, T.—PENELLE, R.: Met. Trans. A., *24A*, 1993, p. 2299.
[28] BAUDIN, T.—JURA, J.—PENELLE, R.—POSPIECH, J.: J. of Appl. Cryst., *28*, 1995, p. 582.
[29] ROUAG, N.—PENELLE, R.: Textures and Microstructures, *11*, 1989, p. 203.
[30] BAUDIN, T.—PAILLARD, P.—PENELLE, R.: Scripta Materialia, *40*, 1999, p. 1111.
[31] HELMING, K.: Texturapproximation durch Modellkomponenten. [Habilitation report]. Clausthal, Germany, Technical University 1995.
[32] JURA, J.: Application of model function in quantitative texture analysis of cubic metals. [Habilitation report]. Krakow, Polish Academy of Sciences, Institute of Metallurgy and Materials Science 1993.
[33] ROUAG, N.: Influence de la texture cristallographique et de la spécialité des joints de grains sur l'anisotropie de migration des joints entourant un grain d'orientation $\{110\}\langle 001\rangle$, au cours des premiers stades de la recristallisation secondaire, dans des tôles de Fe-3%Si, en présence de précipités AlN et MnS. [Thèse de Doctorat d'Etat]. Orsay, France, Université de Paris Sud 1988.
[34] ROE, R. J.: J. Appl. Phys., *36*, 1965, p. 2024.